The effect of magnetocrystalline anisotropy on the domain structure of patterned Fe_2CrSi Heusler alloy thin films

T. Miyawaki,[1,*)] M. Foerster,[2)] S. Finizio,[2)] C. A. F. Vaz,[2,3)] M.-A. Mawass,[2,4)] K. Inagaki,[1)] N. Fukatani,[1)] L. Le Guyader,[5,b)] F. Nolting,[5)] K. Ueda,[1)] H. Asano,[1)] and M. Kläui[2)]

[1]*Department of Crystalline Materials Science, Nagoya University, Nagoya 464-8603, Japan*

[2] *Institut für Physik, Johannes Gutenberg-Universität Mainz, 55099 Mainz, Germany*

[3]*SwissFEL, Paul Scherrer Institut, 5232 Villigen PSI, Switzerland*

[4]*Max Planck Institute for Intelligent Systems, Heisenbergstrasse 3, 70569 Stuttgart, Germany*

[5]*Swiss Light Source, Paul Scherrer Institut, 5232 Villigen PSI, Switzerland*

The effects of magnetic anisotropy on domain structures in half-metallic Heusler alloy Fe_2CrSi thin film elements were investigated using high resolution x-ray magnetic circular dichroism photoemission electron microscopy. The transition of the dominating contribution from the magnetocrystalline anisotropy to the shape anisotropy is observed in square-shaped elements when reducing the size below 2.0-2.5 μm. In particular, we identify in disk-shaped Heusler elements the vortex state as the ground state. The shape-anisotropy dominated, well-defined magnetization configuration shows the potential of the Fe_2CrSi Heusler alloy for applications in vortex-core- or domain-wall-devices, where the high spin polarization is desirable.

a) Electronic: miyawaki@numse.nagoya-u.ac.jp

b) Present address: Helmholtz-Zentrum Berlin für Materialien und Energie GmbH, BESSY II, Albert-Einstein-Strasse 15, 12489 Berlin, Germany

I. INTRODUCTION

Heusler alloys are widely studied since they exhibit a variety of interesting properties such as half-metallic behavior, large magneto-optical constants, and shape memory effects.[1,2] So far, the interest in the research field of spintronics has been focused on cobalt-based ferromagnetic Heusler alloys (Co_2YZ), due to the predicted exciting properties, such as half-metallicity and the high Curie temperature.[3] While much research has been carried out on these Co-based Heusler compounds,[3,4] Fe-based Heusler alloys, such as Fe_2CrSi, promise even better properties for spintronics devices.[5,6] From *ab initio* calculations,[5] Fe_2CrSi presents a spin polarization of 0.98 and in particular has a smaller saturation magnetization, M_s, of 1.98 μ_B/f.u., when compared to the conventional Co-based Heusler alloys (4 ~ 6 μ_B/f.u.).[7,8] Since the critical current for spin transfer switching in magnetic tunnel junctions and the speed of domain wall motion are proportional to M_s and M_s^{-1}, respectively, the small value of M_s in Fe_2CrSi will be an advantage for spin transfer-based switching.[9] The moderately high Curie temperature (630 K) of Fe_2CrSi[6] provides the combination of thermal stability at room temperature with the potential for thermally assisted switching devices.[10] Furthermore, a robustness of the high spin polarization against disorder and temperature is predicted due to a large DOS of majority spins at the Fermi energy.[5]

To utilize these unique material properties of Fe_2CrSi for devices, a detailed knowledge of the domain structure in confined geometries in this material is necessary. In particular it is desirable to tailor the domain structure by varying the geometry, which is possible if the effect of shape anisotropy becomes dominant when reducing the pattern size. Recently, the interplay between shape anisotropy and crystalline anisotropy resulting in well-controlled magnetization configurations has been reported in patterned films made of materials such as Co-based Heusler alloys,[4] $La_{0.7}Sr_{0.3}MnO_3$,[11] and Fe_3O_4[12] probed by high resolution x-ray magnetic circular dichroism photoemission electron microscopy (XMCD-PEEM). Such experiments are necessary as, in contrast to patterned elements in conventional permalloy[13,14,15] where only shape anisotropy acts, the magnetization configurations in these more complex materials is the result of a fine interplay of all the energy terms, including magnetocrystalline anisotropy and shape anisotropy. Particularly, complex magnetic domain structures, such as triangle states and S-states, have been observed in circular elements of Co-based Heusler materials,[4] while for applications the simpler vortex state is more suitable.[16]

So far, neither the magnetocrystalline anisotropy of Fe_2CrSi nor its effect on the magnetic configuration in patterned elements has been reported. We study here the magnetic configuration in patterned thin films of epitaxial Fe_2CrSi by high resolution

XMCD-PEEM imaging. We determine the critical length scale, where the transition between states commensurate with the geometry and states where the intrinsic magnetic materials properties dominate take place, and we find that this transition directly results from the interplay of shape and magnetocrystalline anisotropy. In particular, we identify disks in the vortex state and study the device-relevant behavior in applied fields.

II. EXPERIMENTAL DETAILS

$Fe_2CrSi(t$ nm) was grown on $MgAl_2O_4(001)$ / Fe_2VSi(3 nm) by DC magnetron sputtering at room temperature, followed by a post-annealing at 500 °C for 30 min. The thickness of Fe_2CrSi, t, was varied from 35 nm to 50 nm. As a buffer layer we have used a 3 nm thick Heusler alloy Fe_2VSi grown at 650 °C by DC magnetron sputtering. While Fe_2VSi is an antiferromagnet with a critical temperature of T_N = 123 - 196 K,[17-19] the XMCD-PEEM measurements were performed at room temperature, hence we expect the Fe_2VSi layer not to affect the magnetic properties of the Fe_2CrSi. After the annealing of Fe_2CrSi, a $MgAl_2$ thin film with 0.5 nm thickness is deposited as a capping layer. Focused ion beam (FIB) lithography was used to define micrometer to sub-micrometer scale patterns.

To acquire the magnetic images, the XMCD-PEEM technique was used. We have imaged, exploiting the XMCD effect, the local difference in X-ray absorption and

photoelectron emission at the Fe L_3 edge for left and right circularly polarized X-rays. As, in the XMCD effect, the magnetic contrast depends on the angle between the helicity vector and the magnetization, contrast is maximum when they are parallel or anti-parallel.[20,21] Due to the grazing incidence of the photon beam 16° from the plane, our measurements are mainly sensitive to the in-plane component of the magnetization. X-ray diffraction (XRD) with Cu Kα radiation was used for the structural characterization. Magnetic hysteresis loops of continuous films were measured by vibrating sample magnetometry (VSM).

III. RESULTS AND DISCUSSIONS

Figure 1 shows a $2\theta/\theta$ XRD pattern of a sample with t = 50 nm. Only the (002) and (004) peaks of Fe_2CrSi are visible without any other orientations or secondary phases. The left panel of the inset in Fig. 1 shows ϕ scans of the $MgAl_2O_4$(220) and Fe_2CrSi(220) planes. Both clear four-fold symmetry and in-plane rotation of 45° from the substrate $MgAl_2O_4$(220) are observed in the ϕ scan of Fe_2CrSi(220). From these results, the epitaxial relationship can be identified as $MgAl_2O_4$(001)[100] // Fe_2CrSi(001)[110]. As shown in the right panel of the inset in Fig. 1, (111) peaks were observed, indicating the desired $L2_1$ ordering of the Fe_2CrSi thin film.

Figure 2 shows the magnetic properties of continuous Fe_2CrSi thin films with t = 35

nm, measured using VSM at room temperature. As shown in Fig. 2(a), the direction of the in-plane external magnetic field is measured as the angle θ from the [110] direction of the Fe_2CrSi. Figure 2(b) shows *M-H* loops measured along $\theta = 45°$ and 90°. The saturation magnetization, M_s, is measured to be 410 emu/cm^3, which is close to the calculated M_s of Fe_2CrSi with an $L2_1$ ordered structure (398 emu/cm^3).[5] The ratio M_r/M_s, where M_r stands for the remnant magnetization, for the *M-H* loop at $\theta = 45°$ and 90° show 0.90 and 0.59, respectively. The decrease of magnetization before the field is reversed indicates the rotation of magnetic moments due to crystalline anisotropy. Numerical analysis using the Stoner-Wohlfarth formalism was carried out to determine the crystalline anisotropy constants and the directions of easy axes.[22] From the fitting of the measured hysteresis loops, the four-fold anisotropy and uniaxial anisotropy constants, K_1 and K_u, respectively, were appeared to be K_1 = -266.2 J/m^3 and K_u = 99.8 J/m^3. Since we took $\theta = 0°$ along [110] of Fe_2CrSi, the minus sign of K_1 in this system represent the easy axes of the four-fold anisotropy along [100] and [010]. In Fig. 2(c), the value of M_r/M_s is plotted as a function of θ. The gray line in Fig. 2(c) represents the simulated result using the obtained value of K_1 and K_u, showing a good agreement with the experimental results. From these results, the angular plot is well explained by the combination of four-fold and uniaxial anisotropy; the easy axes of the four-fold

anisotropy are along [100] and [010], while the easy axis of the uniaxial anisotropy is along [110]. The sign of the four-fold crystalline anisotropy constant of the Fe_2CrSi is contrary to Co-based Heusler alloys that show the [110] and [-110] easy axes.[3,22,23] This anisotropy is not due to the Fe_2VSi buffer layer, since the same direction of the easy axes was observed in Fe_2CrSi thin films grown directly on $MgAl_2O_4$ substrates without the Fe_2VSi buffer layers (not shown here). The combination of Fe and Cr at Wyckoff 8c and 4a sites, respectively, may contribute to the anisotropy. However, further research is necessary to understand the difference in the magnetic crystalline anisotropy between Fe_2CrSi and Co-based Heusler alloys. Although a uniaxial anisotropy term is not expected from the point of crystallographic symmetry, it is observed in this study and also in Co-based Heusler alloys.[22,23] One possible explanation for the uniaxial anisotropy is a miscut of the substrates where the step edges can induce additional anisotropies[22,23], but other sources of this anisotropy cannot be ruled out without further structural investigations that are beyond the scope of this work.

Having established the materials parameters, we now turn to the domain structures. The magnetic configurations in square- and disk-shaped Fe_2CrSi thin films obtained from XMCD-PEEM imaging are shown in Fig.3. All the images were taken in remnant states after magnetic saturation with a magnetic field of about 100 mT parallel to the

[110] direction of the Fe_2CrSi, which is also the direction of incidence of the X-rays. In Fig. 3(a), the edges of the square elements are parallel to [100] or [010] of the Fe_2CrSi. All the elements from 3.0 μm to 1.0 μm in size show flux-closure Landau patterns. In these elements, the directions of the easy axes of the magnetocrystalline anisotropy are close to the directions of square edges, which are the easy axes of the shape anisotropy. Therefore, the easy axes of the effective anisotropy, which contains both the magnetocrystalline and the shape anisotropies, are close to the directions of the square edges. As a result, the magnetization in the Fe_2CrSi finds it easy to form the Landau patterns. On the other hand, in Fig. 3(b), where the edges of the squares are parallel to the hard axes of the magnetocrystalline anisotropy, square elements larger than 2.0 ~ 2.5 μm exhibit magnetic S-states.[4] Since the easy axes arising from the shape anisotropy along the square edges are parallel to the hard axes of magnetocrystalline anisotropy, the direction of the square edges are no longer the energy minima for magnetic moments in large structures. By decreasing the element size, shape anisotropy dominates the crystalline anisotropy. The critical size, where the two contributions are energetically equivalent, is around 2.0 μm; smaller (larger) size than this leads to shape (crystalline) anisotropy being dominant. Figure 3(c) shows XMCD-PEEM images of disk-shaped elements with various diameters. In disk-shaped elements having 1.0 to 2.5 μm diameter,

we find the vortex state as the ground state. This is in contrast to the observed behavior in disk elements in Co-based Heusler alloys, where more complex S- and triangular states prevail.[4] The presence of the vortex states in Fe_2CrSi disks is thought to arise from the smaller crystalline anisotropy energy (~4×10^2 J/m^3) of Fe_2CrSi compared to that of Co-based Heusler alloys (more than 10^3 J/m^3),[4,23] indicating that the Fe-based Heusler material can be better suited for devices based on vortices and domain walls where a dominating shape anisotropy is necessary.

Next, we describe our studies on the magnetization process in patterned elements. Figure 4(a) shows magnetic images in disk-shaped Fe_2CrSi thin films with diameters of 2.5 μm (upper panels) and 2.0 μm (lower panels). Images were taken at remnant states after applying a magnetic field. As shown in Fig. 4(a), 2.5 μm diameter disks exhibit the vortex state after applying a field of +15 mT. Subsequently, by gradually applying a negative magnetic field, one finds that the vortex core moves from the left to right hand side of the element. At each step, the vortex core is pinned at off-center positions of the disk, allowing us to observe the vortex core displacement at zero applied field. The pinning of vortex core in the Fe_2CrSi disk is attributed to the effect of magnetocrystalline anisotropy, which generates local minima of the total magnetic energy. Furthermore, local variations in the anisotropy can lead to the creation of

pinning sites. We also find an analogous behavior in the 2.0 μm diameter disk. The direction of movement of the vortex core is opposite to that of the 2.5 μm disk due to the opposite chirality of the vortex state. After applying -10.5 mT, the chirality of the vortex state is reversed, suggesting the vortex core was annihilated while applying the magnetic field and nucleated again when reducing the magnetic field to zero, thus yielding a critical field for expelling the vortex of about 9.0±1.5 mT.

Finally, we investigate in Fig. 4(b) the magnetic configurations in zigzag wires with 0.5 μm, 1.0 μm and 2.0 μm widths as suggested for memory devices.[24,25] After saturation with a large magnetic field (-30 mT), the wires are almost saturated with the magnetization following the wire. However, one can see ripple-like domain structures in some of the wire arms. Since the longitudinal directions of the wires are not parallel to the easy axes of the crystalline anisotropy, the ripple suggests that the effect of crystalline anisotropy on the domain structure cannot be neglected in the wire structures. The 2.0 μm wide wires show a complicated domain structures at +3.0 mT (indicated by circles), followed by complete reversal of magnetization (+4.5 mT and +10.5 mT), showing that these wires are sufficiently wide to allow for the presence of domain walls parallel to the wire (as visible at 3.0 mT). The 1.0 μm and 0.5 μm wires exhibit a reversal by the formation (+3.0 mT and +4.5 mT) and annihilation of head-to-head

domain walls. This can be easily observed, for instance, in the lower panel where the 1.0 μm wide wire is first all dark, then, at 3.0 mT one arm reverses and two head-to-head domain walls are present at the corners. Thus, shape anisotropy governs the magnetic configuration in wires with a width less than 2.0 μm, making these wires suitable for domain-wall devices.

IV. SUMMARY

In summary, we have investigated the interplay between magnetocrystalline and shape anisotropies and the resulting domain structures in FIB-patterned Fe_2CrSi thin films. Epitaxial thin films of Fe_2CrSi with $L2_1$ ordering were grown by magnetron sputtering and the films exhibit a biaxial anisotropy with easy axes along the [100] and [010] directions and a small contribution of a uniaxial anisotropy along [010]. The magnetocrystalline anisotropy energy constants were determined to be $K_1 \sim 4\times10^2$ J/m^3 and $K_u \sim 70$ J/m^3. In patterned elements, a transition from a dominant contribution of the magnetocrystalline anisotropy to a dominant contribution of shape anisotropy is observed when reducing the feature size, with a critical size of the transition around 2.0 to 2.5 μm for the magnetic configurations. We identify the vortex state in disk structures and head-to-head domain walls in wire structures below this lateral size.

These results show the potentials of the Heusler alloy Fe_2CrSi for applications to

spintronics devices: the domain structures can be tailored by the shape anisotropy to yield well-defined vortex and domain wall configurations. Combined with the high spin polarization of the material, these are the necessary prerequisites for its applications in vortex-core and domain wall-based spin torque devices.

ACKNOWLEDGMENTS

This work was funded by MEXT KAKENHI Grant Number 20360005 and 23656214, JSPS KAKENHI Grant Number 24760547, the JSPS Institutional Program for Young Researcher Overseas Visits, the JSPS Young Researcher Overseas Visits Program for Vitalizing Brain Circulation, EUs 7th Framework Programme IFOX (NMP3-LA-2010 246102), MAGWIRE (FP7-ICT-2009-5 257707), the European Research Council through the Starting Independent Researcher Grant MASPIC (ERC-2007-StG 208162), the Graduate School of Excellence “Materials Science in Mainz” (GSC266), the Swiss National Science Foundation, and the DFG. Part of this work was performed at the Swiss Light Source, Paul Scherrer Institut, Villigen, Switzerland.

References

[1]T. Graf, C. Felser, and S. S. P. Parkin, Progr. Solid State Chem. **39**, 1 (2011).

[2]K. H. J. Buschow, P. G. van Engen, and R. Jongebreur, J. Magn. Magn. Mater. **38**, 1 (1983).

[3]S. Trudel, O. Gaier, J. Hamrle, and B. Hillebrands, J. Phys. D: Appl. Phys. **43**, 193001 (2010).

[4]C. A. F. Vaz, J. Rhensius,J. Heidler, P. Wohlhüter, A. Bisig, H. S. Körner, T. O. Mentes, A. Locatelli, L. Le Guyader, F. Nolting, T. Graf, C. Felser, L. J. Heyderman, and M. Kläui, Appl. Phys. Lett. **99**, 182510 (2011).

[5]S. Ishida, S. Mizutani, S. Fujii, and S. Asano, Mater. Trans. **47**, 31 (2006).

[6]S. Yoshimura, H. Asano, Y. Nakamura, K. Yamaji, Y. Takeda, M. Matsui, S. Ishida, Y. Nozaki, and K. Matsuyama, J. Appl. Phys. **103**, 07D716 (2006).

[7]Mahdi Sargolzaei, Manuel Richter, Klaus Koepernik, Ingo Opahle, Helmut Eschrig, and Igor Chaplygin, Phys. Rev. B **74**, 224410 (2006).

[8]I. Galanakis, P. H. Dederichs, and N. Papanikolaou, Phys. Rev. B **66**, 174429 (2002).

[9]A. Thiaville, Y. Nakatani, J. Miltat, and Y. Suzuki, Europhys. Lett. **69**, 990 (2005).

[10]M. H. Kryder, E. C. Gage, T. W. McDaniel, W. A. Challener, R. E. Rottmayer, G. Ju, Y-T. Hsia, and M. F. Erden, Proc. IEEE **96**, 1810 (2008).

[11]J. Rhensius, C. A. F. Vaz, A. Bisig, S. Schweitzer, J. Heidler, H. S. Körner, A. Locatelli, M. A. Niño, M. Weigand, L. Méchin, F. Gaucher, E. Goering, L. J. Heyderman, and M. Kläui, Appl. Phys. Lett. **99**, 062508 (2011).

[12]M. Fonin, C. Hartung, U. Rüdiger, D. Backes, L. Heyderman, F. Nolting, A. Fraile Rodríguez, and M. Kläui, J. Appl. Phys. **109**, 07D315 (2011).

[13]T. Taniuchi, M. Oshima, H. Akinaga, and K. Ono, J. Appl. Phys. **97**, 10J904 (2005).

[14]Jing Shi, S. Tehrani, and M. R. Scheinfein, Appl. Phys. Lett. **76**, 2588 (2000).

[15]M. Kläui and C. A. F. Vaz, *Handbook of Magnetism and Advanced Magnetic Materials*, edited by H. Kronmüller and S. Parkin, (Wiley & Sons, New York, 2007) Vol. 2, p. 879.

[16]Stellan Bohlens, Benjamin Krüger, André Drews, Markus Bolte, Guido Meier, and Daniela Pfannkuche, Appl. Phys. Lett. **93**, 142508 (2008).

[17]K. Endo, H. Matsuda, K. Ooiwa, and K. Itoh, J. Phys. Soc. Jpn, **64**, 2329 (1995).

[18]N. Fukatani, C. Shishikura, Y. Takeda, and H. Asano, Appl. Phys. Express **2**, 053001 (2009).

[19]N. Fukatani, K. Ueda, and H. Asano, J. Appl. Phys. **109**, 073911 (2011).

[20]G Schönhense, J. Phys.: Condens. Matter **11**, 9517 (1999).

[21]J. Stöhr, Y. Wu, B. D. Hermsmeier, M. G. Samant, G. R. Harp, S. Koranda, D. Dunham,

and B. P. Tonner, Science **259**, 658 (1993).

[22]M. S. Gabor, T. Petrisor Jr., C. Tiusan, M. Hehn, and T. Petrisor, Phys. Rev. B **84**, 134413 (2011).

[23]R. Yilgin, Y. Sakuraba, M. Oogane, S. Mizukami, Y. Ando, and T. Miyazaki, Jpn. J. Appl. Phys. **46** L205 (2007).

[24]S. S. P. Parkin, M. Hayashi, and L. Thomas, Science **320**, 190 (2008).

[25]O. Boulle, G. Malinowski, and M. Kläui, Mater. Sci. Eng. R **72**, 159 (2011).

Figure Captions

Fig. 1. (a) Out-of-plane $2\theta/\theta$ XRD pattern of a sample with t = 50 nm. The left panel of the inset shows ϕ scans of $MgAl_2O_4$(220) and Fe_2CrSi(220) planes. The right panel of the inset shows a ϕ scan of the Fe_2CrSi (111) plane.

Fig. 2. Magnetic properties of continuous Fe_2CrSi thin films with t = 35 nm, measured using VSM at room temperature. (a) The direction of the in-plane external magnetic field is given by the angle θ from [110] direction of Fe_2CrSi. (b) *M-H* loops measured at θ = 45° (black squares) and 90° (red triangles). (c) M_r/M_s as a function of θ, where M_r and M_s stand for the saturation magnetization and remnant magnetization, respectively. The angular plot of 180° to 360° is the mirrored one of 0° to 180°. The gray line represents the simulated result. Note that the data is shown between a minimum value of 0.5 (center) and a maximum value of 1 (outermost ring).

Fig. 3. Domain structures in Fe_2CrSi thin film elements obtained from XMCD-PEEM imaging at the Fe L_3 edge. All the images were taken in remnant states after magnetic saturation (with a magnetic field of about 100 mT). (a) The edges of square elements are parallel to [100] or [010] which are the easy axes of Fe_2CrSi. (b) The edges of the

squares are parallel to the hard axes ([110] or [-110]) of the biaxial anisotropy. In (a) and (b), “L” and “S” denoted in the images indicate Landau and S-states, respectively. (c) Disk-shaped elements with various diameters. “V” and “S” denoted in the images indicate vortex and S-states, respectively. The gray scale bars indicate the magnetic contrast direction. In (a) and (b), arrows are plotted in the domain patterns to indicate the directions of magnetization.

Fig. 4 Magnetization process in Fe_2CrSi thin film elements obtained from XMCD-PEEM imaging. Images were taken at remnant states after applying magnetic field. (a) Disk-shaped elements with diameters of 2.5 μm (upper panels) and 2.0 μm (lower panels). (b) Zigzag wires with 0.5 μm, 1.0 μm and 2.0 μm. The wires in upper panels have smaller angles of corners than those in the wires shown in lower panels. In the upper left panel, the crystalline orientation of Fe_2CrSi is denoted. The gray scale bars indicate the magnetic contrast direction.

Fig.1

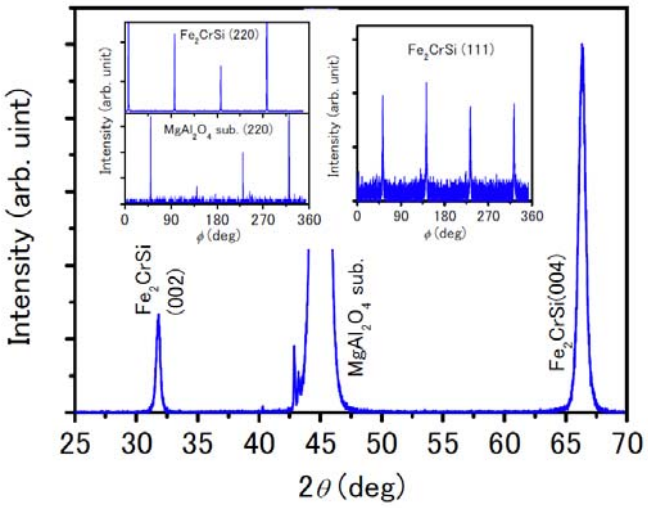
Intensity (arb. uint)
2θ (deg)
Fe2CrSi (002)
MgAl2O4 sub.
Fe2CrSi(004)
Fe2CrSi (220)
MgAl2O4 sub. (220)
Intensity (arb. unit)
φ (deg)
Fe2CrSi (111)

Fig.2

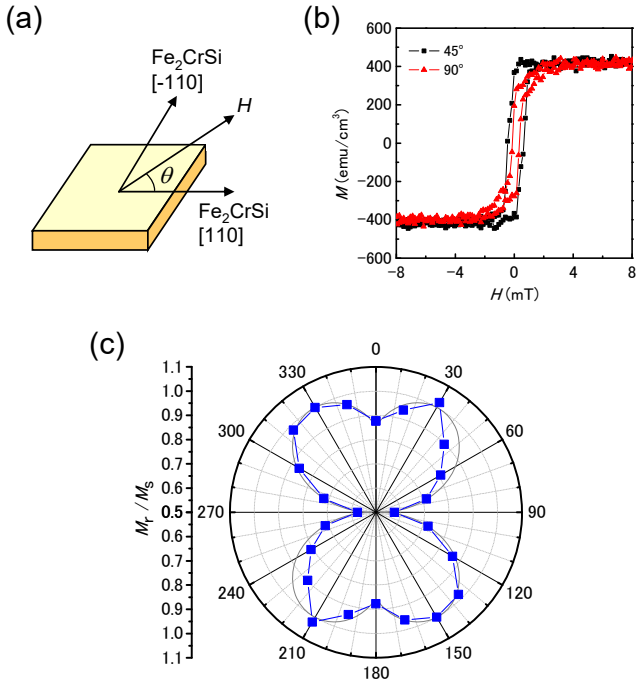

Fig. 3

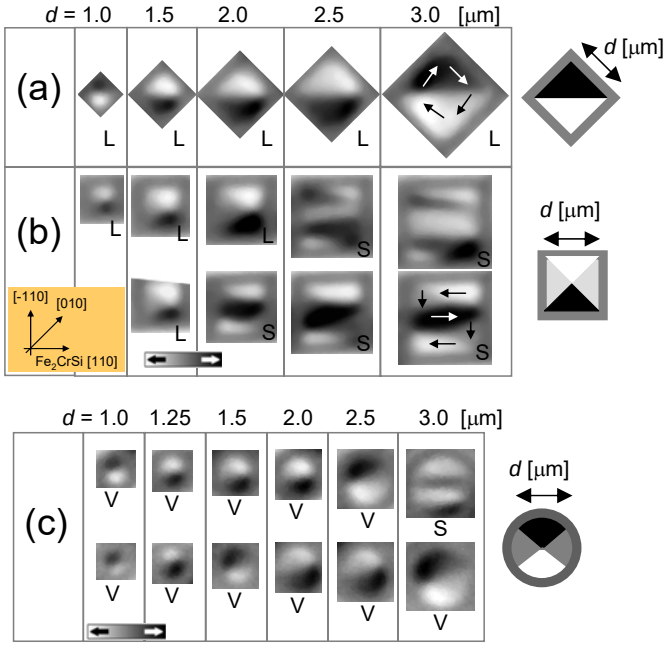
d = 1.0 1.5 2.0 2.5 3.0 [μm]
(a)
L
d [μm]
(b)
S
[-110] [010]
Fe2CrSi [110]
d = 1.0 1.25 1.5 2.0 2.5 3.0 [μm]
(c)
V
S

Fig. 4

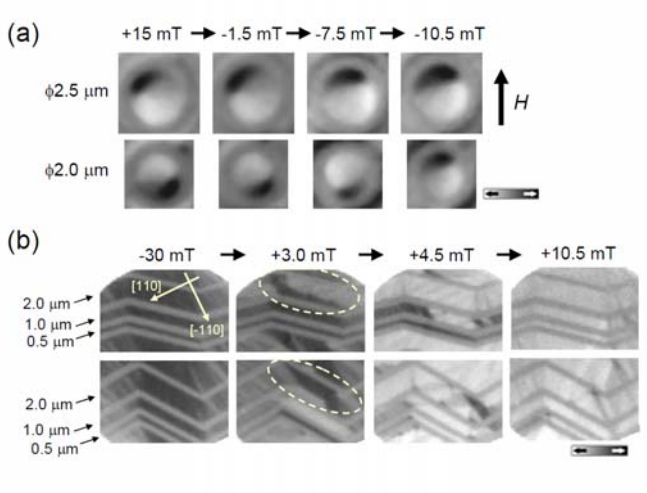
(a)
+15 mT
-1.5 mT
-7.5 mT
-10.5 mT
ϕ2.5 μm
ϕ2.0 μm
H
(b)
-30 mT
+3.0 mT
+4.5 mT
+10.5 mT
[110]
[-110]
2.0 μm
1.0 μm
0.5 μm
2.0 μm
1.0 μm
0.5 μm